Molybdenum-Based Electrode Materials

Subjects: Green & Sustainable Science & Technology

Contributor: Yu Wang , Hai Wang , Gan Qu

As a novel type of green energy storage device, supercapacitors exhibit several orders of magnitude higher capacities than the traditional dielectric capacitors and significantly higher power density than the traditional secondary batteries. Supercapacitors have been widely applied in energy storage fields. Electrode materials, as pivotal components of supercapacitors, play an important role in electrochemical performance. Molybdenum-based materials have attracted widespread attention for their high theoretical capacitance, abundant resources, and facile synthesis tactics. Therefore, it is necessary to systematically summarize the application of Mo-based electrode materials in high-performance supercapacitors and unveil their developmental direction and trends.

supercapacitors Mo-based electrode materials binary materials

1. Introduction

The energy crisis and environmental pollution are the two principal themes in the world. Therefore, renewable clean energy sources, such as wind, solar, and tidal energy, have attracted much attention in the energy fields [1]. However, the development of clean energy is limited by space and time factors [2]. Consequently, effective energy storage systems are needed to promote their commercial application. Among electrochemical energy storage devices, supercapacitors stand out for their high-power density and long cycle life [3][4].

The history of capacitors can be traced back to 1746, while the invention of the Leiden bottle is a pivotal milestone. A typical capacitor comprises two closely aligned conductors separated by an insulating medium. The stored energy of the capacitor is positively related to the voltage until the threshold of breakdown voltage [5]. In 1975, Conway et al. [6] claimed that the charge and discharge behaviors of RuO_2 closely resemble capacitors rather than batteries, and termed them “supercapacitors”.

Supercapacitors can be classified into two main types: electric double layer supercapacitors (EDLCs) and pseudocapacitors. EDLCs stored charge through ion adsorption and desorption on the surface of electrodes. Therefore, EDLCs often show long lifespan and high energy efficiency, because there are only physical reactions on the surface during the charge and discharge processes [7]. In contrast, pseudocapacitive supercapacitors undergo reversible redox reactions in the interior part of the electrode materials [8]. Therefore, pseudocapacitive electrodes often present higher specific capacitance and energy density than those of EDLCs.

Generally, a supercapacitor comprises four components: current collector, electrode, electrolyte, and separator [9]. The electrode material plays a pivotal role in determining the specific capacitance and energy density. As a result,

the design and regulation of electrode materials have become the focus in the field of supercapacitors [10][11][12][13][14].

China is rich in molybdenum resources. The element of Mo exhibits variable valence states (+4, +5, and +6) [15]. In addition, Mo-based materials exhibit pronounced electrochemical activity, which have been widely investigated in recent years [16][17][18]. As shown in **Figure 1**, Mo-based electrode materials can be categorized as binary Mo-based materials (MoO_2, MoO_3), ternary Mo-based materials ($NiMoO_4$, $CoMoO_4$, and $MnMoO_4$, etc.), nanocomposites of Mo-based materials (Mo_2C@CNT and MoS_2/graphene), and Mo-based MOFs and Mo-based materials deriving from MOF materials (Mo-MOF/PANI and BiMo-MOF).

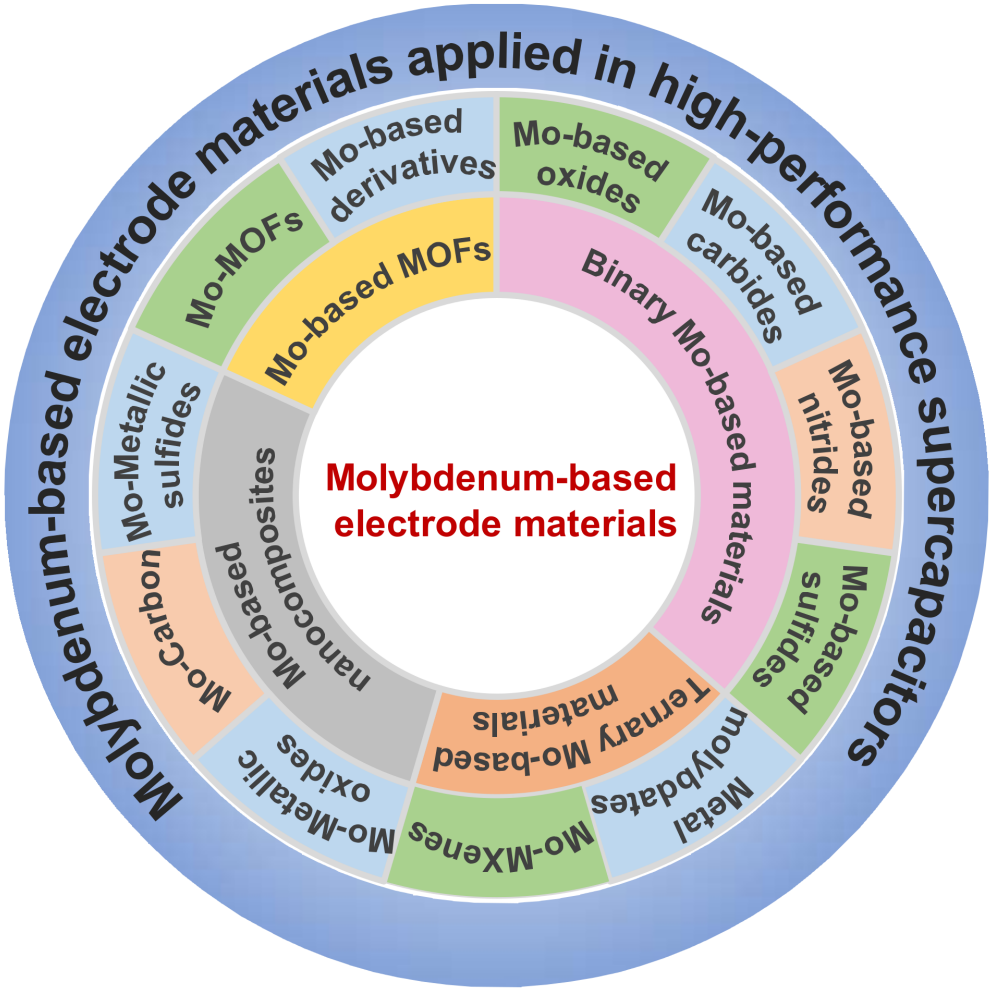

Figure 1. A series of Mo-based electrode materials for supercapacitors.

2. Mo-Based Electrode Materials for Supercapacitors

2.1. Binary Mo-Based Materials

Binary Mo-based materials are composed of two different types of elements, for example MoO_3, Mo_2C, MoN, and MoS_2, etc., which have attracted extensive research into supercapacitors.

2.1.1. Molybdenum Oxides

Molybdenum oxides mainly include MoO_2, MoO_3, and MoO_{3-x}, which are composed of MoO_6 octahedra through edge or corner sharing [19].

MoO_3 usually exists in three crystal types: α-MoO_3, β-MoO_3, and h-MoO_3. α-MoO_3 belongs to the orthorhombic crystal system, in which MoO_6 octahedra are connected with each other through weak van der Waals forces along the [010] direction and corner sharing along the [100] direction [20]. β-MoO_3 belongs to the monoclinic crystal system, in which MoO_6 octahedra are connected through corner sharing [21]. h-MoO_3 belongs to the hexagonal crystal system, in which MoO_6 octahedra share edges along the [001] direction and corners along the [100] direction [22]. Therefore, h-MoO_3 shows a zig-zag structure with a cavity of ~3 Å in diameter allowing for the insertion/deinsertion of ions [23]. Prakash et al. [24] employed the solution combustion method to synthesize a series of α-MoO_3 nanorods at different combustion temperatures. The SEM image in **Figure 2**a illustrates the morphology of α-MoO_3, which shows one-dimensional nanorods with a diameter of 50 nm and length of several micrometers. The α-MoO_3 nanorods show a specific capacitance of 176 F g^{-1} at 1 mA g^{-1}. Even after 1000 cycles, the capacitance retention reaches 92%. Additionally, Niu et al. [25] synthesized the h-MoO_3 nanorods and nanoparticles using a hydrothermal method, as shown in **Figure 2**b. The nanorod structure facilitates adequate contact between the electrode materials and electrolyte, thereby improving the electrochemical performance. As a result, the MoO_3 nanorods achieved a specific capacitance of 229.0 F g^{-1} at 0.2 A g^{-1}. Zhu et al. [26] fabricated MoO_3 nanoplates by the heat-treating of C_3N_4 and ammonium molybdate (**Figure 2**c). The extended layered structure enables the rapid insertion/deinsertion of ions. Notably, a high specific capacitance of 994.2 F g^{-1} was achieved at 0.5 A g^{-1}. Moreover, the assembled YP50//MoO_3 device shows a capacitance retention of 84% after 1500 cycles at 3 A g^{-1}.

MoO_2 belongs to the monoclinic crystal system, in which the twisted MoO_6 octahedra units are connected to each other along the [001] direction by sharing edges. The distorted structure induces a change in the electronic state of Mo, leading to metallic conductivity [27]. Ma et al. [28] synthesized MoO_2 nanoparticles using a hydrothermal method (**Figure 2**d) and explored their electrochemical behavior in acid electrolytes. The charge storage behavior of MoO_2 under acidic conditions is ascribed to the surface redox reactions (Faradaic capacitance) and ion intercalation/deintercalation reactions (battery capacitance). However, the electrochemical mechanism of MoO_2 is ascribed to the electric double layer capacitors' behavior under the neutral electrolyte. Notably, the MoO_2 electrode exhibited a specific capacitance of 509.8 F g^{-1} at 0.5 A g^{-1} in a 0.5 M H_2SO_4 solution. Additionally, the morphological structure of MoO_2 is also investigated to improve its capacitive performance. Wu et al. [29] synthesized hierarchical mesoporous MoO_2 spheres using a hydrothermal method (**Figure 2**e). The MoO_2 nanospheres exhibit a specific surface area of 29.5 m^2 g^{-1}, facilitating ion contact and improvement in charge transfer resistance. As a result, the specific capacitance reaches 381.0 F g^{-1} at 0.3 A g^{-1}. Furthermore, the crystal structure of MoO_2 is further researched to reveal its influence on the performance of supercapacitors. Zhao et al. [30] introduced amorphous domains into MoO_2 nanosheets (**Figure 2**f), which enhances the ion diffusion and electron transport. Under a current density of 5 A g^{-1}, the capacitance retention remains 85% after 4000 cycles.

Non-stoichiometric MoO_{3-x}($0 < x < 1$) enhances the intrinsic conductivity and increases the concentration of free carriers due to the introduced oxygen vacancies [31]. In comparison with MoO_3 (3.2 eV), the bandgap of MoO_{3-x} is reduced to 2.9 eV, which is expected to favor improved capacitance performance [32]. There have been many strategies to construct MoO_{3-x}. In addition, the size and shape adjustment of oxygen-deficient molybdenum oxides is relatively mature. At present, the reported methods mainly include the template method [33], surfactant method [34], solvothermal method [35], and sol–gel method [36], etc. Wu et al. [35] successfully synthesized MoO_{3-x} nanobelts with oxygen vacancy concentration of up to 20%. **Figure 2**g illustrates the MoO_{3-x} nanobelts, which show 30–40 nm in thickness and 100–200 nm in width. This structural design reduces the migration distance of electrolyte ions and enhances the availability of internal active sites. Notably, the MoO_{3-x} nanobelt exhibits a remarkable specific capacitance of 1,220 F g^{-1} at 50 A g^{-1} and shows an impressive capacitance retention of nearly 100% even after 38,000 cycles. Bai et al. [37] synthesized α-MoO_{3-x} nanobelts via a facile one-pot hydrothermal approach (**Figure 2**h). The enlarged interlayer spacing could weaken the interlamellar Van der Waals force, facilitating the rapid diffusion of ions. The α-MoO_{3-x} nanobelts exhibit a specific capacitance of 912.5 F g^{-1} at 1 A g^{-1}. Salkar et al. [38] synthesized two-dimensional MoO_{3-x} microplates and microdisks. The SEM images illustrate the morphological structures in **Figure 2**i. According to the experimental data, the improved capacitor performance stems from the introduction of oxygen vacancies, the high specific surface area, and the enlarged layered structures. The MoO_{3-x} microplates and microdisks display specific capacitances of 410 F g^{-1} and 226 F g^{-1} at 20 A g^{-1}, respectively. Impressively, the capacitance retention is above 90% and the coulombic efficiency is above 98% after 10,000 cycles.

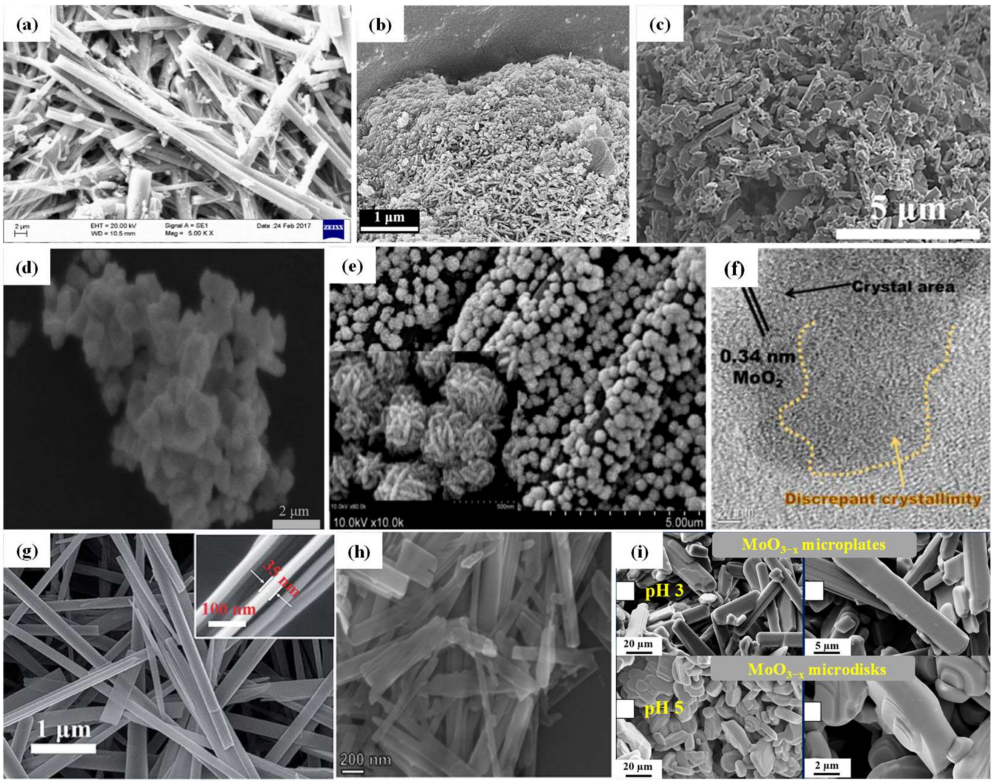

Figure 2. SEM images. (**a**) MoO_3 nanorods. (**b**) h-MoO_3 nanorods and nanoparticles. (**c**) MoO_3 nanoplates. (**d**) MoO_2 nanoparticles. (**e**) Mesoporous MoO_2 spheres. (**f**) MoO_2 nanosheets. (**g**) MoO_{3-x} nanobelts. (**h**) MoO_{3-x}

nanobelts. (**i**) MoO_{3-x} microplates and microdisks.

2.1.2. Molybdenum Carbides

Transition metal carbides (TMCs) possess high electrical conductivity, and have been widely studied in energy storage, catalysis, and electromagnetic shielding fields. Now, the reported TMCs mainly include NbC [39], VC [40], TiC [41], and Mo_2C [42], etc. Notably, Mo_2C has been widely investigated in supercapacitors.

Yu et al. [43] conducted simulation calculations to analyze the electronic properties of molybdenum carbide. The energy band structure and projected DOS are presented in **Figure 3**a. For the molybdenum carbides (MoC, Mo_2C, MoC_2), an increase in the proportion of C means a reduction in free electrons on the surface. Mo_2C with the smallest proportion of C and numerous dangling bonds on the surface shows significant potential as an electrode material in supercapacitors. Illustrated in **Figure 3**b, Xu et al. [42] successfully synthesized lamellar Mo_2C through the calcination of amine–metal oxides, yielding ultrafine nanoparticles of ~10 nm. This microstructural design is beneficial for the adequate contact between the electrode and electrolyte, facilitating improved performance. Remarkably, a specific capacitance of 88 F g^{-1} has been achieved at 0.5 A g^{-1}. In addition, the asymmetric Mo_2C//AC capacitor displays an impressive capacitance retention of 95% after 1200 cycles and an energy density of 44.1 W h kg^{-1}.

2.1.3. Molybdenum Nitrides

Transition metal nitrides (TMNs) have received extensive attention in the energy storage and catalysis fields due to their high electrical conductivity and robust chemical stability [44]. Xiao et al. [45] employed the salt template method to synthesize MoN nanosheets, as demonstrated in **Figure 3**c. The MoN nanosheets exhibit a negligible band gap and an exceptional electronic conductivity, thereby improving the electrochemical performance. Notably, the volume-specific capacitance reaches 928 F cm^{-3} at 2 mV s^{-1}, while maintains 200 F cm^{-3} even under 20 mV s^{-1}. Gao et al. [46] prepared zig-zag γ-Mo_2N thin film by magnetron sputtering. The SEM image is presented in **Figure 3**d. The zig-zag structured γ-Mo_2N presents an outstanding area capacitance of 248 mF cm^{-2} at 50 mV s^{-1}. After 20,000 cycles at 200 mV s^{-1}, a remarkable capacitance retention of 95% is achieved. In addition, the symmetrical solid-state γ-Mo_2N//γ-Mo_2N device delivers an excellent power density of 107.1 W cm^{-3} at 33.8 mW h cm^{-3}. Djire et al. [47] synthesized face-centered cubic γ-Mo_2N with high surface area through high-temperature treatment of molybdenum source and ammonia gas, as illustrated in **Figure 3**e. The pseudocapacitive charge storage mechanism was conducted through in situ experiments. As a result, the simultaneous insertion of hydrogen ions (H^+) and electrons (e^-) into the material leads to the reduction in Mo during the electrochemical processes. The γ-Mo_2N shows a high specific capacitance of 1500 F g^{-1} with a potential window of 1.2 V in aqueous acidic electrolytes.

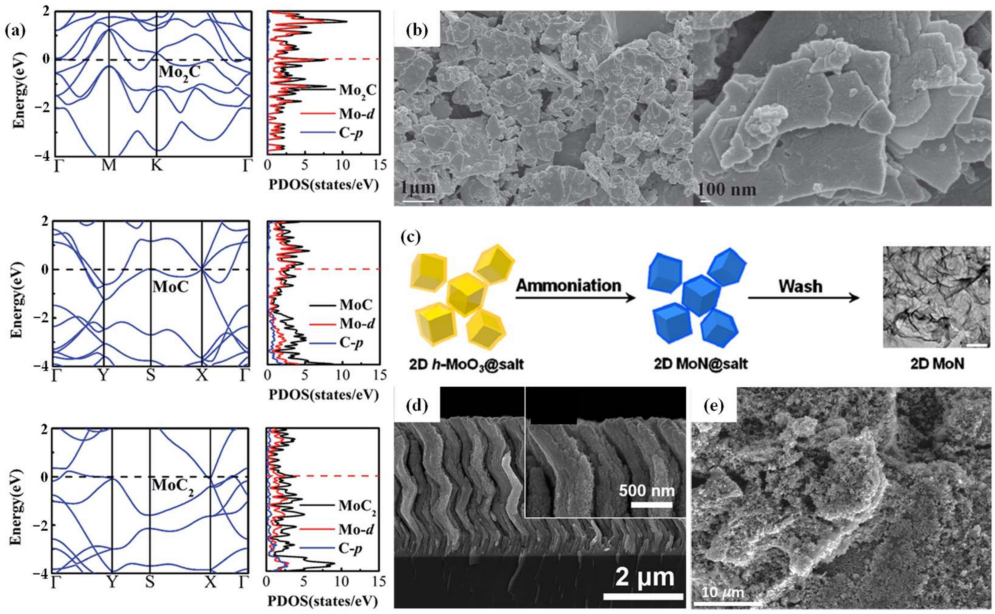

Figure 3. (**a**) Calculated band structures and projected DOS for Mo_2C, MoC, and MoC_2. (**b**) SEM image of Mo_2C nanosheets. (**c**) Schematic diagram of the synthesis of MoN nanosheets. (**d**) SEM image of zig-zag γ-Mo_2N films. (**e**) SEM image of γ-Mo_2N.

2.1.4. Molybdenum Sulfides

Molybdenum chalcogenides possess a layered structure, in which the large interlayer spaces are convenient for the storage and transport of ions [48]. This layered characteristic renders them an ideal candidate as an energy storage material. Molybdenum sulfide (MoS_2) and molybdenum selenide ($MoSe_2$) stand out in molybdenum chalcogenides. The high intrinsic ionic conductivity facilitates improved electrochemical performance. MoS_2 displays layered S-Mo-S stacks under van der Waals interactions [49]. There are two distinct phase states: the metallic 1T phase and the semiconducting 2H phase. The 1T phase easily transforms into the 2H phase due to its thermodynamic instability. MoS_2 predominantly exists in the form of the 2H phase in nature [50]. The active sites of the 2H phase are mainly distributed along the sulfur edge, while those of the metallic 1T phase are mainly distributed along both the edge and basal plane, inherently favoring the electrochemical process [51].

Liu et al. [52] used a simple one-step hydrothermal method to obtain rosette-like MoS_2 nanoflowers (**Figure 4**a). **Figure 4**b presents the GCD curves of MoS_2 nanoflowers at varying current densities; they exhibit a specific capacitance of 137 mF cm^{-2} at 10 mA cm^{-2}. After 10,000 cycles, the capacitance retention reaches 81.6%. Teli et al. [53] reported amorphous MoS_2 nanoflakes (**Figure 4**c) using one-step electrodeposition, achieving a specific capacitance of 416.9 mF cm^{-2} at 1 mA cm^{-2}. An asymmetric device was assembled using activated carbon and MoS_2 as negative and positive electrodes, respectively; this exhibited an area capacitance of 277.3 mF cm^{-2} and energy density of 0.15 mW h cm^{-2} at 5.33 mW cm^{-2}. Furthermore, 90.1% cyclability and excellent coulombic efficiency measured up to 3000 cycles were observed for an asymmetric device (**Figure 4**d). Additionally, Joseph et al. [54] prepared defect-rich 1T-MoS_2 nanosheets, which exhibited a specific capacitance of 379 F g^{-1} at a current density of 1 A g^{-1}. The assembled supercapacitor device delivered an energy density of 21.3 W h kg^{-1} and

a power density of 750 W kg^{-1}. The capacitance retention remains 92% even after 3000 cycles (**Figure 4**e). Gupta et al. [55] utilized a hydrothermal method to synthesize MoS_2 nanoflowers. The surface features of the flakes and wrinkles facilitate the intercalation and deintercalation of cations. Notably, a specific capacitance of 255.65 F g^{-1} is achieved at a current density of 0.25 A g^{-1}. Impressively, even after 1000 cycles, 70% of the initial specific capacitance is retained (**Figure 4**f).

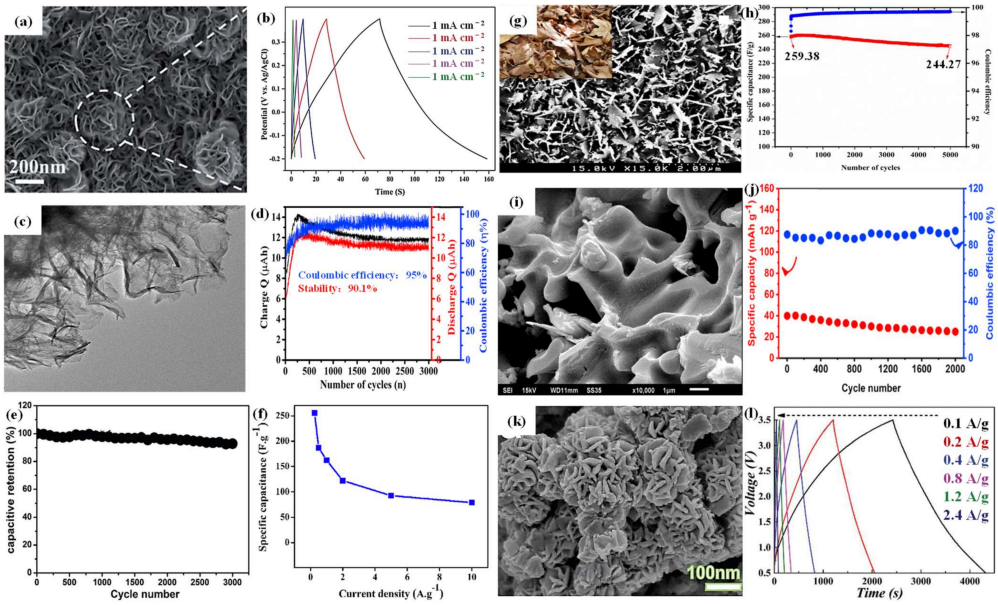

Figure 4. (**a**) SEM image of MoS_2 nanoflowers; (**b**) GCD curves of MoS_2 nanoflowers at different current densities. (**c**) TEM image of MoS_2 nanoflakes; (**d**) cyclic performance of MoS_2 nanoflakes at 3 mA cm^{-2}. (**e**) Cyclic performance of 1T-MoS_2 nanosheets at 5 A g^{-1}. (**f**) Specific capacitance of MoS_2 nanoflowers at different current densities. (**g**) SEM image of mesoporous $MoSe_2$; (**h**) cyclic performance of mesoporous $MoSe_2$ at 1 A g^{-1}. (**i**) SEM image of 2H-$MoSe_2$; (**j**) cyclic performance of 2H-$MoSe_2$ at 5 A g^{-1}. (**k**) SEM image of $MoSe_2$ nanoflowers; (**l**) CV curves of $MoSe_2$ nanoflowers at different current densities.

The atomic structure of $MoSe_2$ closely resembles that of MoS_2, comprising three atomic layers held together by weak van der Waals interactions. Consequently, $MoSe_2$ has attracted considerable interest as a potential electrode material in supercapacitors [56].

$MoSe_2$ with a mesoporous structure shows a large specific surface area, providing significant benefits for ion transport. Vattikuti et al. [57] successfully synthesized a uniform dry leaf-like mesoporous $MoSe_2$ nanostructure using a microwave-assisted method, as illustrated in **Figure 4**g. The as-prepared leaf-like perforated $MoSe_2$ exhibited remarkable capacitance of 257.38 F g^{-1} at 1 A g^{-1} with a capacitance retention of almost 95% after 5000 cycles, see **Figure 4**h. In comparison to the mesoporous configuration, $MoSe_2$ with a nanosheet structure further increases the specific surface area, shortens the ion diffusion path, and improves the electrochemical performance. Upadhyay et al. [58] reported the synthesis of layered 2H-$MoSe_2$ nanosheets via an in situ selenization route. The SEM image is shown in **Figure 4**i. The $MoSe_2$ nanosheet exhibits a specific capacitance of 46.22 mA h g^{-1} at 2 A g^{-1}. Remarkably, even after 2000 cycles at a current density of 5 A g^{-1}, a capacitance retention of 64% was

observed (**Figure 4**j). Additionally, the nanoflower structure would offer ample channels for electrolyte diffusion during the electrochemical processes. Zhang et al. [59] synthesized smooth and irregular pleated flower-like $MoSe_2$ using a facile hydrothermal method. The SEM image is displayed in **Figure 4**k. Furthermore, **Figure 4**l illustrates the CV curves of $MoSe_2$ at different current densities. Notably, the specific capacitance reaches 641.5 mA h g^{-1} at a current density of 0.1 A g^{-1}. The assembled hybrid $MoSe_2$//AC capacitors displayed a high energy density of 78.75 W h kg^{-1} and a high power density of 3600 W kg^{-1}. In addition, the capacity retention rate is 70.28% after 5000 cycles with a potential window of 0.5–3.5 V.

2.2. Ternary Mo-Based Materials

Ternary Mo-based materials are composed of three elements, including metal molybdates and MXenes. The synthesis pathway of metal molybdate is simple and low cost while exhibiting remarkable physical and chemical properties [60]. MXenes exhibit a characteristic two-dimensional layered structure, offering a high specific surface area and exceptional electrical conductivity [61]. Notably, ternary Mo-based materials have been widely researched for supercapacitors in recent years.

2.2.1. Metal Molybdates

Metal molybdates, for example $MMoO_4$ (M = Cu [62], Zn [63], Bi [64], Ni [65], Mn [66], Sn [67], Co [68], etc.), constitute a significant category in inorganic materials.

Farahpour et al. [62] conducted a single-pot hydrothermal method to grow $CuMoO_4$ nanosheets on nickel foam. In **Figure 5**a, the prepared $CuMoO_4$ nanosheets are uniformly distributed with grass-like morphology. The specific capacitance of $CuMoO_4$ reached 2259.55 F g^{-1} at 1 A g^{-1}. The cyclic stability analysis showed a capacitance retention of 90.08% at 16 A g^{-1} after 5000 cycles. Moreover, the $CuMoO_4$//AC supercapacitor device displayed a high energy density of 52.51 W h kg^{-1} at 600 W kg^{-1}. In addition, the device exhibited a capacitance retention of 78.6% after 5000 cycles at 4 A g^{-1} (**Figure 5**b). Gurusamy et al. [63] produced a series of rod-shaped $ZnMoO_4$ using a template method by optimizing the concentration of CTAB. The schematic diagram of the synthesis process is presented in **Figure 5**c. The rod-like $ZnMoO_4$ material showed an impressive specific capacitance of 779 F g^{-1} at 5 mV s^{-1} and retained 90% of the initial capacitance even after 3000 cycles at 100 mV s^{-1}. Additionally, Yesuraj et al. [64] employed the hydrothermal method with a DNA template to synthesize Bi_2MoO_6 nanoplates, as depicted in **Figure 5**d. The Bi_2MoO_6 nanoplates with a large number of small nanoparticles (5–7 nm) on their surface result in an increased surface area, which facilitated charge transport and ion diffusion. The Bi_2MoO_6 exhibited a high specific capacitance of 698 F g^{-1} at 5 mV s^{-1}, along with a capacitance retention of 86% even after 3000 cycles at a high scan rate of 100 mV s^{-1} in 1 M NaOH electrolyte. Qu et al. [65] presented a rapid and zero-energy consumption method to obtain metal molybdate nanowires in supercapacitors (**Figure 5**e). The synthesized $NiMoO_4$ nanowires exhibited an impressive specific capacitance of 549 C g^{-1} at 1 A g^{-1}. Furthermore, the assembled supercapacitor device demonstrated a specific capacitance of 156 F g^{-1} at 0.8 A g^{-1}, along with an energy density of 55.6 W h kg^{-1} at 640 W kg^{-1}. Additionally, Sheng et al. [66] employed a solid-state chemical synthesis approach to produce 1D $MnMoO_4$ $0.9H_2O$ and $MnMoO_4$ nanorods (**Figure 5**f), which exhibited a specific

capacitance of 210.2 F g^{-1} at 1 A g^{-1}. Notably, the $MnMoO_4$ nanorods displayed remarkable cycle stability, maintaining a cycle life of 112.6% even after 10,000 cycles. Furthermore, the electrochemical performance of $MnMoO_4$ underwent substantial enhancement upon the removal of crystal water from $MnMoO_4{\cdot}0.9H_2O$, leading to a noteworthy 2.4-fold increase in specific capacitance. Remarkably, the asymmetric supercapacitor device achieved a high energy density of 23.5 W h kg^{-1} at 187.4 W kg^{-1}. This remarkable electrochemical performance is attributed to the elevated electrical conductivity from the 1D nanostructure after the removal of crystallization water. Sakthikumar et al. [67] optimized the ratio of CTAB to metal salt and reaction conditions to synthesize sheet-like $Sn(MoO_4)_2$, as shown in the SEM image in **Figure 5**g. The specific capacitance of flake $Sn(MoO_4)_2$ is 109 F g^{-1} at 5 mV s^{-1} and the capacitance retention reaches 70% after 4000 cycles at 8 mV s^{-1}. Li et al. [68] synthesized $CoMoO_4$ material in situ on nickel foam using a hydrothermal method (**Figure 5**h). The prepared $CoMoO_4$ shows a cuboid rod-like structure with loose folds on the periphery, enhancing the contact between the electrode and electrolyte, and thereby facilitating ion diffusion and transmission. At a current density of 3 mA cm^{-2}, the discharge capacitance of $CoMoO_4$ reaches 11.112 F cm^{-2}.

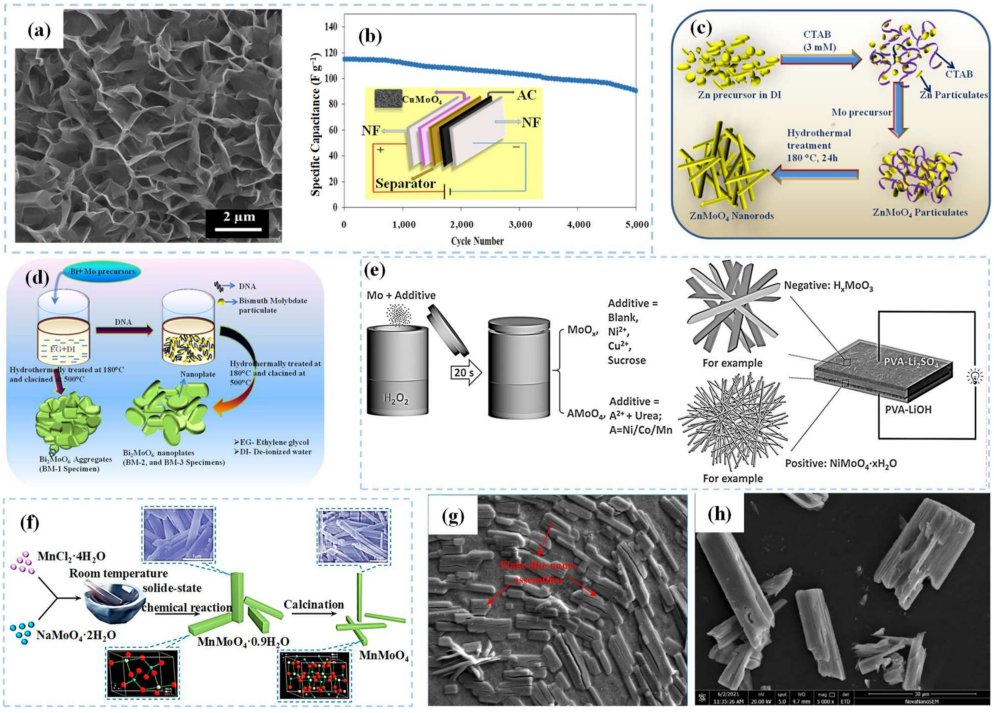

Figure 5. (**a**) SEM image of $CuMoO_4$ nanosheets; (**b**) cyclic performance of $CuMoO_4$//AC at 4 A g^{-1}. (**c**) Schematic diagram of the synthesis of $ZnMoO_4$ nanorods. (**d**) Schematic diagram of the synthesis of Bi_2MoO_6 nanoplates. (**e**) Schematic diagram of the synthesis of $NiMoO_4{\cdot}xH_2O$ nanowires. (**f**) Schematic diagram of the synthesis of $MnMoO_4$ nanorods. (**g**) SEM image of $Sn(MoO_4)_2$ nanosheets. (**h**) SEM image of $CoMoO_4$ nanorods.

2.2.2. Mo-MXenes

In recent years, two-dimensional transition metal carbonitride (MXene) materials have attracted extensive attention in the energy storage field, owing to their unique physical and chemical characters [69]. The MAX phase is classified as a layered carbide or nitride and is characterized by the chemical formula $M_{n+1}AX_n$ (n = 1~3). Here, M represents

various transition metal elements, including Sc, Ti, Zr, Nb, Ta, Cr, Mo, etc. X stands for carbon and/or nitrogen, while A refers to a main group element. Through etching, A can be removed from the MAX phase, leading to the formation of a graphene-like MXene structure. The structural chemical formula of MXenes is $M_{n+1}X_nT_x$ (n = 1~3), where T represents a functional group such as O, F, or OH [70]. The distinctive properties of MXene materials have sparked interest from researchers in supercapacitors.

Halim et al. [71] firstly put forward a large-scale synthesis strategy for 2D Mo_2CT_x flakes. LiF/HCl acts as an etchant to selectively etch Ga from Mo_2Ga_2C powder, leading to a delamination process, as depicted in **Figure 6**a. The obtained Mo_2CT_x flakes exhibit high conductivity and effective intersheet conduction due to their dense stacking. At a scan rate of 2 mV s^{-1}, the specific capacitance reaches 700 F cm^{-3}, while the capacitance retention is nearly 100% even after 10,000 cycles at 10 A g^{-1} (**Figure 6**b). Das et al. [72] conducted a theoretical analysis on the structure of Mo_2CO_2 to predict the electronic structure and investigate its capacitive behavior. As a result, the functionalized MXenes induce a change in charge transfer dynamics. Therefore, H inclines to form covalent bonds with O, leading to the sharing of electrons. Impressively, the theoretically calculated capacitance of Mo_2CO_2 is closely consistent with the experimental results. Zheng et al. [73] prepared $Mo_{1.33}CT_z$ i-MXene films with a vacancy structure by etching $(Mo_{0.66}Sc_{0.33})_2AlC$, as illustrated in **Figure 6**c. The inclusion of vacancies notably optimizes the ion transport. Notably, the $Mo_{1.33}CT_z$ i-MXene attained an energy density of 25.4 mW h cm^{-3} at a power density of 152.4 mW cm^{-3} in a 15 M LiBr electrolyte, as depicted in **Figure 6**d. Even after 20,000 cycles at 100 mV s^{-1}, 99.4% of the initial specific capacitance is retained (**Figure 6**e).

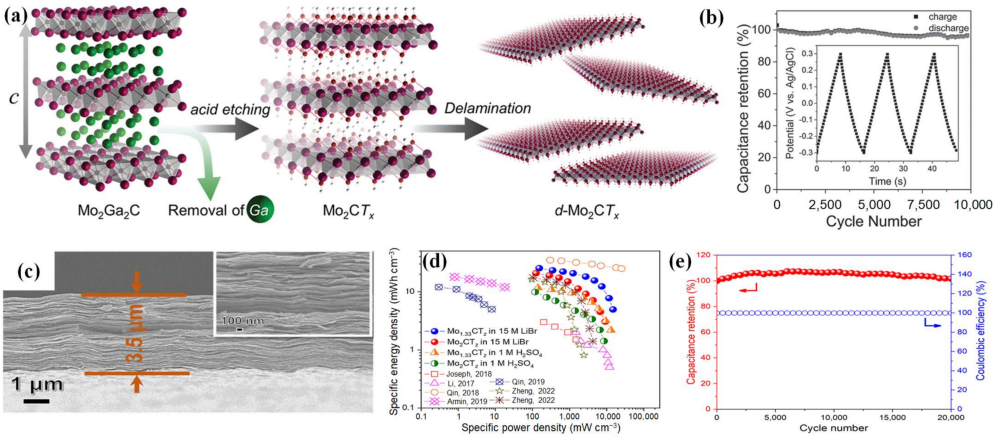

Figure 6. (**a**) Schematic diagram of the synthesis of Mo_2CT_x; (**b**) cyclic performance of Mo_2CT_x at 10 A g^{-1}. (**c**) SEM image of $Mo_{1.33}CT_z$; (**d**) Ragone diagram of $Mo_{1.33}CT_z$ in 1 M H_2SO_4 and 15 M LiBr compared to different Mxene; (**e**) cyclic performance of $Mo_{1.33}CT_z$ at 100 mV s^{-1}.

References

1. Song, D.; Liu, Y.; Qin, T.; Gu, H.; Cao, Y.; Shi, H. Overview of the policy instruments for renewable energy development in China. Energies 2022, 15, 6513.

2. Pan, Y.; Dong, F. Dynamic evolution and driving factors of new energy development: Fresh evidence from China. Technol. Forecast. Soc. Chang. 2022, 176, 14.
3. Guo, L.; Hu, P.; Wei, H. Development of supercapacitor hybrid electric vehicle. J. Energy Storage 2023, 65, 8.
4. Lamba, P.; Singh, P.; Singh, P.; Singh, P.; Bharti; Kumar, A.; Gupta, M.; Kumar, Y. Recent advancements in supercapacitors based on different electrode materials: Classifications, synthesis methods and comparative performance. J. Energy Storage 2022, 48, 103871.
5. Frackowiak, E.; Abbas, Q.; Béguin, F. Carbon/carbon supercapacitors. J. Energy Chem. 2013, 22, 226–240.
6. Conway, B.E. Transition from “supercapacitor” to “battery” behavior in electrochemical energy storage. J. Electrochem. Soc. 1991, 138, 1539–1548.
7. Ji, H.; Zhao, X.; Qiao, Z.; Jung, J.; Zhu, Y.; Lu, Y.; Zhang, L.L.; MacDonald, A.H.; Ruoff, R.S. Capacitance of carbon-based electrical double-layer capacitors. Nat. Commun. 2014, 5, 3317.
8. Lu, X.F.; Wang, A.L.; Xu, H.; He, X.J.; Tong, Y.X.; Li, G.R. High-performance supercapacitors based on MnO2 tube-in-tube arrays. J. Mater. Chem. A 2015, 3, 16560–16566.
9. Sharma, S.; Chand, P. Supercapacitor and electrochemical techniques: A brief review. Results Chem. 2023, 5, 100885.
10. Kumar, S.; Saeed, G.; Zhu, L.; Hui, K.N.; Kim, N.H.; Lee, J.H. 0D to 3D carbon-based networks combined with pseudocapacitive electrode material for high energy density supercapacitor: A review. Chem. Eng. J. 2021, 403, 126352.
11. Wang, D.; Tang, K.; Xiao, J.; Li, X.; Long, M.; Chen, J.; Gao, H.; Chen, W.; Liu, C.; Liu, H. Advances of electrospun Mo-based nanocomposite fibers as anode materials for supercapacitors. Sustain. Mater. Technol. 2021, 29, e00302.
12. Xiong, C.; Zhang, Y.; Xu, J.; Dang, W.; Sun, X.; An, M.; Ni, Y.; Mao, J. Kinetics process for structure-engineered integrated gradient porous paper-based supercapacitors with boosted electrochemical performance. Nano Res. 2023, 16, 9471–9479.
13. Xiong, C.; Zheng, C.; Jiang, X.; Xiao, X.; Wei, H.; Zhou, Q.; Ni, Y. Recent progress of green biomass based composite materials applied in supercapacitors, sensors, and electrocatalysis. J. Energy Storage 2023, 72, 108633.
14. Xiong, C.; Wang, T.; Han, J.; Zhang, Z.; Ni, Y. Recent research progress of paper-based supercapacitors based on cellulose. Energy Environ. Mater. 2023, e12651.
15. Mendoza-Sánchez, B.; Brousse, T.; Ramirez Castro, C.; Nicolosi, V.; Grant, P.S. An investigation of nanostructured thin film α-MoO3 based supercapacitor electrodes in an aqueous electrolyte. Electrochim. Acta 2013, 91, 253–260.

16. Ma, H.; Liang, J.; Qiu, J.; Jiang, L.; Ma, L.; Sheng, H.; Shao, M.; Wang, Q.; Li, F.; Fu, Y.; et al. A biocompatible supercapacitor diode with enhanced rectification capability toward ion/electron-coupling logic operations. Adv. Mater. 2023, 35, e2301218.
17. Vikraman, D.; Hussain, S.; Karuppasamy, K.; Santhoshkumar, P.; Kathalingam, A.; Jung, J.; Kim, H.S. Fabrication of asymmetric supercapacitors using molybdenum dichalcogenide nanoarray structures. Int. J. Energy Res. 2022, 46, 18410–18425.
18. Yuksel, R.; Coskun, S.; Unalan, H.E. Coaxial silver nanowire network core molybdenum oxide shell supercapacitor electrodes. Electrochim. Acta 2016, 193, 39–44.
19. Saji, V.S.; Lee, C.W. Molybdenum, molybdenum oxides, and their electrochemistry. ChemSusChem 2012, 5, 1146–1161.
20. Mai, L.Q.; Hu, B.; Chen, W.; Qi, Y.Y.; Lao, C.S.; Yang, R.S.; Dai, Y.; Wang, Z.L. Lithiated MoO3 nanobelts with greatly improved performance for lithium batteries. Adv. Mater. 2007, 19, 3712–3716.
21. De Castro, I.A.; Datta, R.S.; Ou, J.Z.; Castellanos Gomez, A.; Sriram, S.; Daeneke, T.; Kalantar-Zadeh, K. Molybdenum oxides—From fundamentals to functionality. Adv. Mater. 2017, 29, 31.
22. Huang, C.; Zhang, W.; Zheng, W. The debut and spreading the landscape for excellent vacancies-promoted electrochemical energy storage of nano-architected molybdenum oxides. Mater. Today Energy 2022, 30, 101154.
23. Pan, W.; Tian, R.; Jin, H.; Guo, Y.; Zhang, L.; Wu, X.; Zhang, L.; Han, Z.; Liu, G.; Li, J.; et al. Structure, optical, and catalytic properties of novel hexagonal metastable h-MoO3 nano- and microrods synthesized with modified liquid-phase processes. Chem. Mater. 2010, 22, 6202–6208.
24. Prakash, N.G.; Dhananjaya, M.; Narayana, A.L.; Shaik, D.P.M.D.; Rosaiah, P.; Hussain, O.M. High performance one dimensional α-MoO3 nanorods for supercapacitor applications. Ceram. Int. 2018, 44, 9967–9975.
25. Niu, Y.; Li, X.; Su, H.; Li, J.; Qi, Y. Formation of three dimensional porous h-MoO3 architecture and its application in supercapacitors. Mater. Lett. 2022, 316, 132062.
26. Zhu, Y.; Tan, Y.; Li, H. MoO3 nanoplates preparation via self-sacrifice C3N4 for supercapacitors in an acid electrolyte. J. Energy Storage 2023, 60, 106657.
27. Hao, J.; Zhang, J.; Xia, G.; Liu, Y.; Zheng, Y.; Zhang, W.; Tang, Y.; Pang, W.K.; Guo, Z. Heterostructure manipulation via in situ localized phase transformation for high-rate and highly durable lithium ion storage. ACS Nano 2018, 12, 10430–10438.
28. Ma, B.; Hao, W.; Ruan, W.; Yuan, C.; Wang, Q.; Teng, F. Unveiling capacitive behaviors of MoO2 in different electrolytes and flexible MoO2-based asymmetric micro-supercapacitor. J. Energy Storage 2022, 52, 104833.

29. Wu, K.; Zhao, J.; Zhang, X.; Zhou, H.; Wu, M. Hierarchical mesoporous MoO2 sphere as highly effective supercapacitor electrode. J. Taiwan Inst. Chem. Eng. 2019, 102, 212–217.
30. Zhao, X.; Wang, H.E.; Cao, J.; Cai, W.; Sui, J. Amorphous/crystalline hybrid MoO2 nanosheets for high-energy lithium-ion capacitors. Chem. Commun. 2017, 53, 10723–10726.
31. Luo, Z.; Miao, R.; Huan, T.D.; Mosa, I.M.; Poyraz, A.S.; Zhong, W.; Cloud, J.E.; Kriz, D.A.; Thanneeru, S.; He, J.; et al. Mesoporous MoO3–x material as an mfficient mlectrocatalyst for hydrogen evolution reactions. Adv. Energy Mater. 2016, 6, 11.
32. Gurusamy, L.; Karuppasamy, L.; Anandan, S.; Liu, N.; Lee, G.J.; Liu, C.H.; Wu, J.J. Enhanced performance of charge storage supercapattery by dominant oxygen deficiency in crystal defects of 2-D MoO3-x nanoplates. Appl. Surf. Sci. 2021, 541, 148676.
33. Kuwahara, Y.; Furuichi, N.; Seki, H.; Yamashita, H. One-pot synthesis of molybdenum oxide nanoparticles encapsulated in hollow silica spheres: An efficient and reusable catalyst for epoxidation of olefins. J. Mater. Chem. A 2017, 5, 18518–18526.
34. Li, X.; Wang, D.; Zhang, Y.; Liu, L.; Wang, W. Surface-ligand protected reduction on plasmonic tuning of one-dimensional MoO3−x nanobelts for solar steam generation. Nano Res. 2020, 13, 3025–3032.
35. Wu, Q.L.; Zhao, S.X.; Yu, L.; Zheng, X.X.; Wang, Y.F.; Yu, L.Q.; Nan, C.W.; Cao, G.Z. Oxygen vacancy-enriched MoO3-x nanobelts for asymmetric supercapacitors with excellent room/low temperature performance. J. Mater. Chem. A 2019, 7, 13205–13214.
36. Cong, S.; Hadipour, A.; Sugahara, T.; Wei, T.; Jiu, J.; Ranjbar, S.; Hirose, Y.; Karakawa, M.; Nagao, S.; Aernouts, T.; et al. Modifying the valence state of molybdenum in the efficient oxide buffer layer of organic solar cells via a mild hydrogen peroxide treatment. J. Mater. Chem. C 2017, 5, 889–895.
37. Bai, Y.; Ma, Y.; Zheng, S.; Zhang, C.; Hu, C.; Liang, B.; Xu, Y.; Huang, G.; Yang, R. Oxygen deficiency and single-crystalline MoO3−x nanobelt as advanced supercapacitor negative electrode and dye adsorbent. Colloids Surf. A 2022, 647, 129064.
38. Salkar, A.V.; Naik, A.P.; Peña, G.D.J.G.; Bharath, G.; Haija, M.A.; Banat, F.; Morajkar, P.P. 2D α-MoO3-x truncated microplates and microdisks as electroactive materials for highly efficient asymmetric supercapacitors. J. Energy Storage 2022, 48, 103958.
39. Cao, Y.B.; Zhi, S.X.; Qi, H.B.; Zhang, Y.; Qin, C.; Yang, S.P. Evolution behavior of ex-situ NbC and properties of Fe-based laser clad coating. Opt. Laser Technol. 2020, 124, 8.
40. Gao, J.; Xu, C.; Tian, X.; Sun, M.; Zhao, J.; Ma, J.Y.; Zhou, H.; Xiao, J.; Wu, M. Design bifunctional vanadium carbide embedded in mesoporous carbon electrode for supercapacitor and dye-sensitized solar cell. Sol. Energy 2020, 206, 848–854.

41. Wan, C.; Zhang, R.; Wang, S.; Liu, X. Molten salt electrolytic fabrication of TiC-CDC and its applications for supercapacitor. J. Mater. Sci. Technol. 2017, 33, 788–792.
42. Xu, Y.; Yang, Q.Q.; Zhang, W.B.; Liu, M.C.; Kong, L.B. Enhanced performance for a high electrical conductive Mo2C electrode based proton ionic liquid electrolytes in supercapacitors. Mater. Res. Express 2018, 5, 75508.
43. Yu, Y.; Guo, Z.; Peng, Q.; Zhou, J.; Sun, Z. Novel two-dimensional molybdenum carbides as high capacity anodes for lithium/sodium-ion batteries. J. Mater. Chem. A 2019, 7, 12145–12153.
44. Luo, Q.; Lu, C.; Liu, L.; Zhu, M. A review on the synthesis of transition metal nitride nanostructures and their energy related applications. Green Energy Environ. 2023, 8, 406–437.
45. Xiao, X.; Yu, H.; Jin, H.; Wu, M.; Fang, Y.; Sun, J.; Hu, Z.; Li, T.; Wu, J.; Huang, L.; et al. Salt-templated synthesis of 2D metallic MoN and other nitrides. ACS Nano 2017, 11, 2180–2186.
46. Gao, Z.; Zhang, T.; Wang, Q.; Heinz Mayrhofer, P. Nanostructured zig-zag γ-Mo2N thin films produced by glancing angle deposition for flexible symmetrical solid-state supercapacitors. Mater. Des. 2023, 225, 111432.
47. Djire, A.; Siegel, J.B.; Ajenifujah, O.; He, L.; Thompson, L.T. Pseudocapacitive storage via micropores in high-surface area molybdenum nitrides. Nano Energy 2018, 51, 122–127.
48. Wang, L.; Liu, X.; Luo, J.; Duan, X.; Crittenden, J.; Liu, C.; Zhang, S.; Pei, Y.; Zeng, Y.; Duan, X. Self-Optimization of the Active Site of Molybdenum Disulfide by an Irreversible Phase Transition during Photocatalytic Hydrogen Evolution. Angew. Chem. Int. Ed. 2017, 56, 7610–7614.
49. Li, R.; Liang, S.; Aihemaiti, A.; Li, S.; Zhang, Z. Effectively enhanced piezocatalytic activity in flower-like 2H-MoS2 with tunable S vacancy towards organic pollutant degradation. Appl. Surf. Sci. 2023, 631, 157461.
50. Marinov, A.D.; Bravo Priegue, L.; Shah, A.R.; Miller, T.S.; Howard, C.A.; Hinds, G.; Shearing, P.R.; Cullen, P.L.; Brett, D.J.L. Ex situ characterization of 1T/2H MoS2 and their carbon composites for energy applications, a review. ACS Nano 2023, 17, 5163–5186.
51. Li, H.; Han, X.; Jiang, S.; Zhang, L.; Ma, W.; Ma, R.; Zhou, Z. Controllable fabrication and structure evolution of hierarchical 1T-MoS2 nanospheres for efficient hydrogen evolution. Green Energy Environ. 2022, 7, 314–323.
52. Liu, X.; Liu, L.; Wu, Y.; Wang, Y.; Yang, J.; Wang, Z. Rosette-like MoS2 nanoflowers as highly active and stable electrodes for hydrogen evolution reactions and supercapacitors. RSC Adv. 2019, 9, 13820–13828.
53. Teli, A.M.; Beknalkar, S.A.; Mane, S.M.; Bhat, T.S.; Kamble, B.B.; Patil, S.B.; Sadale, S.B.; Shin, J.C. Electrodeposited crumpled MoS2 nanoflakes for asymmetric supercapacitor. Ceram. Int. 2022, 48, 29002–29010.

54. Joseph, N.; Muhammed Shafi, P.; Chandra Bose, A. Metallic 1T-MoS2 with defect induced additional active edges for high performance supercapacitor application. N. J. Chem. 2018, 42, 12082–12090.

55. Gupta, H.; Chakrabarti, S.; Mothkuri, S.; Padya, B.; Rao, T.N.; Jain, P.K. High performance supercapacitor based on 2D-MoS2 nanostructures. Mater. Today Proc. 2020, 26, 20–24.

56. Sha, R.; Maity, P.C.; Rajaji, U.; Liu, T.-Y.; Bhattacharyya, T.K. Review—MoSe2 nanostructures and related electrodes for advanced supercapacitor developments. J. Electrochem. Soc. 2022, 169, 13503.

57. Vattikuti, S.V.P.; Devarayapalli, K.C.; Nagajyothi, P.C.; Shim, J. Microwave synthesized dry leaf-like mesoporous MoSe2 nanostructure as an efficient catalyst for enhanced hydrogen evolution and supercapacitor applications. Microchem. J. 2020, 153, 104446.

58. Upadhyay, S.; Pandey, O.P. Synthesis of layered 2H-MoSe2 nanosheets for the high-performance supercapacitor electrode material. J. Alloys Compd. 2021, 857, 157522.

59. Zhang, H.-J.; Wang, Y.-K.; Kong, L.-B. A facile strategy for the synthesis of three-dimensional heterostructure self-assembled MoSe2 nanosheets and their application as an anode for high-energy lithium-ion hybrid capacitors. Nanoscale 2019, 11, 7263–7276.

60. Zhang, L.; Zheng, S.; Wang, L.; Tang, H.; Xue, H.; Wang, G.; Pang, H. Fabrication of metal molybdate micro/nanomaterials for electrochemical energy storage. Small 2017, 13, 19.

61. Yang, J.; Yao, G.; Sun, S.; Chen, Z.; Yuan, S.; Wu, K.; Fu, X.; Wang, Q.; Cui, W. Structural, magnetic properties of in-plane chemically ordered (Mo2/3R)2AlC (R=Gd, Tb, Dy, Ho, Er and Y) MAX phase and enhanced capacitance of Mo1.33C MXene derivatives. Carbon 2021, 179, 104–110.

62. Farahpour, M.; Arvand, M. Single-pot hydrothermal synthesis of copper molybdate nanosheet arrays as electrode materials for high areal-capacitance supercapacitor. J. Energy Storage 2021, 40, 102742.

63. Gurusamy, H.; Sivasubramanian, R.; Johnbosco, Y.; Bhagavathiachari, M. Morphology-controlled synthesis of one-dimensional zinc molybdate nanorods for high-performance pseudocapacitor electrode application. Chem. Pap. 2020, 75, 1715–1726.

64. Yesuraj, J.; Austin Suthanthiraraj, S.; Padmaraj, O. Synthesis, characterization and electrochemical performance of DNA-templated Bi2MoO6 nanoplates for supercapacitor applications. Mater. Sci. Semicond. Process. 2019, 90, 225–235.

65. Qu, G.; Li, T.; Jia, S.; Zheng, H.; Li, L.; Cao, F.; Wang, H.; Ma, W.; Tang, Y.; Wang, J. Rapid and scalable synthesis of Mo-based binary and ternary oxides for electrochemical applications. Adv. Funct. Mater. 2017, 27, 1700928.

66. Sheng, R.; Hu, J.; Lu, X.; Jia, W.; Xie, J.; Cao, Y. Solid-state synthesis and superior electrochemical performance of MnMoO4 nanorods for asymmetric supercapacitor. Ceram. Int. 2021, 47, 16316–16323.
67. Sakthikumar, K.; Ede, S.R.; Mishra, S.; Kundu, S. Shape-selective synthesis of Sn(MoO4)2 nanomaterials for catalysis and supercapacitor applications. Dalton Trans. 2016, 45, 8897–8915.
68. Li, L.; Zhou, J.; Zhang, Y.; Pei, X. Synthesis process optimization and electrochemical properties of CoMoO4 supercapacitor prepared by in situ growth method. J. Mater. Sci. Mater. Electron. 2022, 33, 23851–23866.
69. Liang, C.; Meng, Y.; Zhang, Y.; Zhang, H.; Wang, W.; Lu, M.; Wang, G. Insights into the impact of interlayer spacing on MXene-based electrodes for supercapacitors: A review. J. Energy Storage 2023, 65, 20.
70. Garg, R.; Agarwal, A.; Agarwal, M. A review on MXene for energy storage application: Effect of interlayer distance. Mater. Res. Express 2020, 7, 21.
71. Halim, J.; Kota, S.; Lukatskaya, M.R.; Naguib, M.; Zhao, M.Q.; Moon, E.J.; Pitock, J.; Nanda, J.; May, S.J.; Gogotsi, Y.; et al. Synthesis and characterization of 2D molybdenum carbide (MXene). Adv. Funct. Mater. 2016, 26, 3118–3127.
72. Das, M.; Ghosh, S. Theoretical investigation of capacitances in functionalised MXene supercapacitors Mn+1CnO2, M. = Ti, V., Nb, Mo. J. Phys. D Appl. Phys. 2021, 55, 85502.
73. Zheng, W.; Halim, J.; Persson, P.O.Å.; Rosen, J.; Barsoum, M.W. Effect of vacancies on the electrochemical behavior of Mo-based MXenes in aqueous supercapacitors. J. Power Sources 2022, 525, 231064.